catalysts

MDPI

Article

Preparing Cu_2O/Al_2O_3 Coating via an Electrochemical Method for the Degradation of Methyl Orange in the Process of Catalytic Wet Hydrogen Peroxide Oxidation

De-bo Liu [1,*], Ping Zhang [2] and Jian Wang [2]

[1] Faculty of Engineering, Huanghe Science and Technology College, No. 666 Zijingshan South Road, Zhengzhou 450063, China
[2] Institute of Intelligent Manufacturing, Xinxiang Vocational and Technical College, Xinxiang 453006, China
* Correspondence: ldb@hhstu.edu.cn

Abstract: To improve the catalytic efficiency and decrease the reaction temperature of wet air oxidation technology, a Cu_2O/Al_2O_3 coating was prepared on the surface of aluminium alloys by anodizing technology, and subsequent heating treatment. Then, the Cu_2O/Al_2O_3 coating and 3 wt.% H_2O_2 was used to degrade methyl orange. The influence of the coating's microstructure, crystalline component on the degradation rate of the methyl orange was studied. The microstructure of the coating was observed by scanning electron microscope. Results proved that the coating was composed of micropores, and Cu_2O was evenly dispersed on the surface and pores in the Al_2O_3 coating. X-ray diffraction pattern analysis demonstrated Cu_2O and Al_2O_3 characteristic peaks were found after the coating was treated at 300 °C, showing that amorphous Cu_2O and Al_2O_3 were transformed into crystalline oxide. A UV-vis spectrophotometer was used to measure the absorbance of methyl orange, and it was found that the maximum absorption wavelength of methyl orange is 460 nm. At that wavelength, the suitable degradation condition of methyl orange was studied, and results showed that when electrochemical deposition time was 30 min and catalyst dosage was 8 g, the degradation rate of methyl orange could reach 92% at 25 °C for 120 min. Furthermore, when the catalyst was reused 9 times, the degradation rate still reached 75%. Based on the above results, a kinetic equation between the degradation rate of methyl orange and catalyst dosage was derived. The microstructure and crystalline component of the catalyst after different reuse times were characterized, and results showed that the catalytic efficiency of the Cu_2O/Al_2O_3 coating decreased with a decrease in the coating's specific surface area and the ratio of Cu_2O in the coating.

Keywords: Cu_2O/Al_2O_3 coating; degradation; catalytic wet hydrogen peroxide oxidation; electrochemical deposition; anodizing

Citation: Liu, D.-b.; Zhang, P.; Wang, J. Preparing Cu_2O/Al_2O_3 Coating via an Electrochemical Method for the Degradation of Methyl Orange in the Process of Catalytic Wet Hydrogen Peroxide Oxidation. *Catalysts* **2022**, *12*, 1308. https://doi.org/10.3390/catal12111308

Academic Editors: Filippo Bossola and Nicola Scotti

Received: 10 July 2022
Accepted: 19 September 2022
Published: 25 October 2022

1. Introduction

Dyes have the characteristics of high organic content, high salinity, complex composition, high chromaticity, and poor biodegradability. They enrich color but damage the environment [1]. Most of these dyes are toxic, non-biodegradable and carcinogenic due to their large size and complex structure. In fact, most dyes are composed of thiocarboxylic acid groups, nitro groups, carboimino groups, and especially azo groups, which are difficult to degrade. Azo dyes have high toxicity and are harmful to various water microorganisms, fish species. Furthermore, they cause serious damage to the humans, including damage to kidneys, the reproductive system, liver, brain, and central nervous system they are exposed to azo dyes for a long time. Azo dyes are known to be mutagens and carcinogens due to the presence of amines, and related metabolites. Thus, the treatment of azo dyes wastewater has become an urgent problem [2]. Because their accumulation creates potential risks and threats to aquatic organisms and human being [3], studying an effective treatment for azo dye wastewater has become a great challenge to researchers all over the world [4–6].

Many methods, such as adsorption [7], membrane separation [8], extraction [9], chemical oxidation [10], coagulation [11], wet air oxidation [12], photocatalytic oxidation [13], and microbial degradation [14], can be adopted to degrade azo wastewater. Wet air oxidation technology (WAO) is an advanced oxidation technology developed during the last century that is suitable for treating harmful, and toxic wastewater. However, the degradation of pollutants is often carried out at high temperature and high pressure, and high operating costs and low degradation efficiency limit its application. The standard oxide electrode potential of OH is 2.80 V, as H_2O_2 can produce OH, which has a strong oxidative capacity to degrade pollutants. Therefore, during the WAO process, adding H_2O_2 can improve the degradation efficiency of pollutants. However, the addition of H_2O_2 cannot decrease the activation energy of degradation, and the service life of ·OH is short. As a result, the degradation efficiency cannot satisfy requirements for pollution treatment [15]. If a suitable catalyst is mixed during the WAO process, the activation energy of the reaction can be reduced, and the pollutants can be completed degraded in a shorter time and under milder conditions. Therefore, the catalytic wet hydrogen oxidation method (CWPO) was studied to improve the WAO technology [16]. Due to the strong oxidative capacity of OH and low activation energy, the CWPO method has moderate reaction conditions, short treatment periods, and low treatment cost. The catalyst's activity and selectivity can be adjusted to degrade different organic matters. According to the status of the catalyst, the CWPO process can be divided into homogeneous and heterogeneous degradation processes [17]. Soluble Cu, Fe, Ni and Mn salts have been used as catalysts for degradation of wastewater. In this process, the CWPO process is homogeneous reaction, and the Fenton oxidation method is used most to degrade dye wastewater [18]. When solid catalysts are used to decompose H_2O_2, OH is generated to degrade organic matters and the CWPO process is a heterogeneous reaction [19]. In the homogeneous process, the active components of the catalyst can be dissolved in the wastewater, but this decreases the catalytic activity and causes secondary pollution. Compared with the homogeneous process, the heterogeneous process does not require subsequent treatments, and has therefore received extensive attention [20].

The reaction process of CWPO can be seen in Table 1, and it consists of three stages [21], in the process of CWPO, preparation of a suitable catalyst is key to improving the degradation efficiency of pollutants.

Table 1. The reaction process of CWPO.

Initiation of chain	$RH + O_2 \rightarrow R\cdot + HOO$ (RH represents organic matter)	(1)
	$2RH + O_2 \rightarrow 2R\cdot + H_2O_2$	(2)
	$H_2O_2 + M \rightarrow 2OH\cdot$ (M represents catalyst)	(3)
Development or transmission of chain	$RH + \cdot OH \rightarrow R\cdot + H_2O$	(4)
	$R\cdot + O_2 \rightarrow ROO\cdot$	(5)
	$ROO\cdot + RH \rightarrow ROOH + R\cdot$	(6)
Termination of chain	$R\cdot + R\cdot \rightarrow R\text{-}R$	(7)
	$ROO\cdot + R\cdot \rightarrow ROOR$	(8)
	$ROO\cdot + ROO\cdot \rightarrow ROH + RCOR_2 + O_2$	(9)

Compared with precious metals [22,23] and rare earths [24], Cu-based catalysts have higher activity and a lower price. Due to its uneven atomic distribution, high specific surface area, excellent physicochemical properties, and the occurrence of wide range of oxidation states of copper, copper and copper (I) oxide nanoparticles have diverse activity and promote several types of reactions including oxidations, reductions, cross coupling, A3 coupling, electrocatalysis and photocatalysis [25]. The reaction mechanism of Cu-based catalysts is similar to that of Fe^{3+}/Fe^{2+} catalysts during the CWPO process, but their kinetic constants are 4–5 orders of magnitude higher than that of the Fenton reaction [26]. Therefore, a Cu-based catalyst can produce more OH faster, and the degradation efficiency of dye pollutants can be improved. The intermediate products of dye wastewater degradation are organic acids. The pH range of a Cu-based catalyst is wider than that of an iron-based catalyst, and the complexes between organic acids and a Cu-based catalyst are decomposed

more easily compared to those of an Fe-based catalyst. Therefore, Cu-based catalysts are better in obtaining a complete degradation product, and have become the most promising catalysts in the process of CWPO [27]. As nano Cu (I) oxide has several active sites and oxygen vacancies, and can also adsorb and excite O_2 as a highly active oxygen species, it has higher activity than micron Cu (I) oxide [28]. However, nano Cu (I) oxide is easily washed away and agglomerated, and suffers from photo-wavering and photo-corrosion, which limits its application [29]. When it is supported on the surface of porous materials, such as γ-Al_2O_3 [30], TiO_2 coatings [31], activated carbon [32], and porous polymers [33], the process of wastewater treatment can be simplified, and its service life can be prolonged. To reduce the particle size and improve the stability of nano Cu, Cu (I) oxide [34], and composite oxides [35] can be used. Because γ-Al_2O_3 has a high specific surface area, and good thermal stability and mechanical stability, it is widely used as a carrier in various catalysts. Because γ-Al_2O_3 has both acidic and alkaline centers and an activated H-H, C-H bond, it can provide active components to a variety of catalytic reactions, and can also be used as a bifunctional catalyst [36]. γ-Al_2O_3 has tetrahedral structure, which can enhance catalytic activity by forming a composite oxide with Cu (I) oxide. When Cu (I) oxide is loaded with γ-Al_2O_3, the oxygen atom of the Cu (I) oxide interacts with a tricoordinated Al atom. When each Cu atom attaches to a tricoordinated O atom bound to hexacoordinated Al atoms, the Cu-O distance and Cu-O-Cu angle are changed, and the catalytic activity of Cu (I) oxide can be improved [37]. Therefore, using Cu_2O/γ-Al_2O_3 to degrade dye wastewater has received extensive attention [38,39].

In the process of CWPO, H_2O_2 is used to promote the degradation of pollutants. Normally, the degradation efficiency of pollutants increases with increased temperature. However, the decomposition rate of H_2O_2 also increases with increased reaction temperature. Therefore, degradation should be conducted at room temperature. Highly dispersed Cu (I) oxide is easily agglomerated, so improving the degradation efficiency and stability of the Cu_2O/γ-Al_2O_3 catalyst is a challenge in the CWPO process. Using aluminium alloys as the anode, in H_2SO_4 solution, an anodic coating with a regular porous structure can be prepared easily on the surface [40]. This sample can be employed as the cathode, and Cu used as the anode. In the same electrolyte, Cu (I) oxide can be deposited in the holes on the surface of aluminium alloys uniformly [41]. Although the Al_2O_3 and Cu_2O in the coating are amorphous, they can be transformed into crystalline structures by a heating method [42]. The crystalline transformation temperature for amorphous alumina into γ-Al_2O_3 is 300 °C [43], thus, the heating temperature is set at 300 °C. Based on the above, to enhance the efficiency and stability of a Cu_2O/Al_2O_3 catalyst, a Cu_2O/Al_2O_3 coating was prepared by an electrochemical method. The aperture distribution of the coatings was analyzed by scanning electron microscopy (SEM) and Image J software. The crystalline composition of the catalyst was studied by energy dispersive spectrometer (EDS), an X-ray diffractometer (XRD), and X-ray photoelectron spectroscopy (XPS). The catalytic efficiency and stability of a Cu_2O/Al_2O_3 coating on methyl orange was studied by UV-Vis spectroscopy (UV-Vis) at room temperature.

2. Results and Discussion

2.1. Microstructure of the Cu_2O/Al_2O_3 Coating

After the samples were anodized at a current density of 50 mA/cm^2, reaction temperature of 4 °C for 40 min in 10 wt.% H_2SO_4 solution and with electrochemical deposition for 30 min, the micro surface and cross-section of the Cu_2O/Al_2O_3 coating without and with heating temperatures of 200, 300, and 400 °C were studied by scanning electron microscopy. Results are shown in Figure 1. After the treatment, there was a Cu_2O/Al_2O_3 coating on the surface of aluminium alloys, and the coating was closely bonded with the substrate. Figure 1a,c,e,g shows that the heating treatment increased the number of micropores on the surface. However, with increase in heating temperature, microcracks on the surface increased. Moreover, the coating thickness became uneven, which would lead to the catalyst being easier to separate from the substrate and decrease the catalytic activity of the

Cu_2O/Al_2O_3 coating. Figure 1b,d,f,h shows that there were through-pores in the coating, and with the increased heating temperature, the pore sizes increased. As methyl orange is organic, with a benzene ring and the azo bond, it is effective only when the pore size is big enough. When the heating temperature was 200 °C, the pore size was too small. When the heating temperature was 400 °C, there were too many cracks in the coating, and when the heating temperature was 300 °C, there were few cracks and a suitable pore size, which could enhance the catalytic activity of the Cu_2O/Al_2O_3 coating.

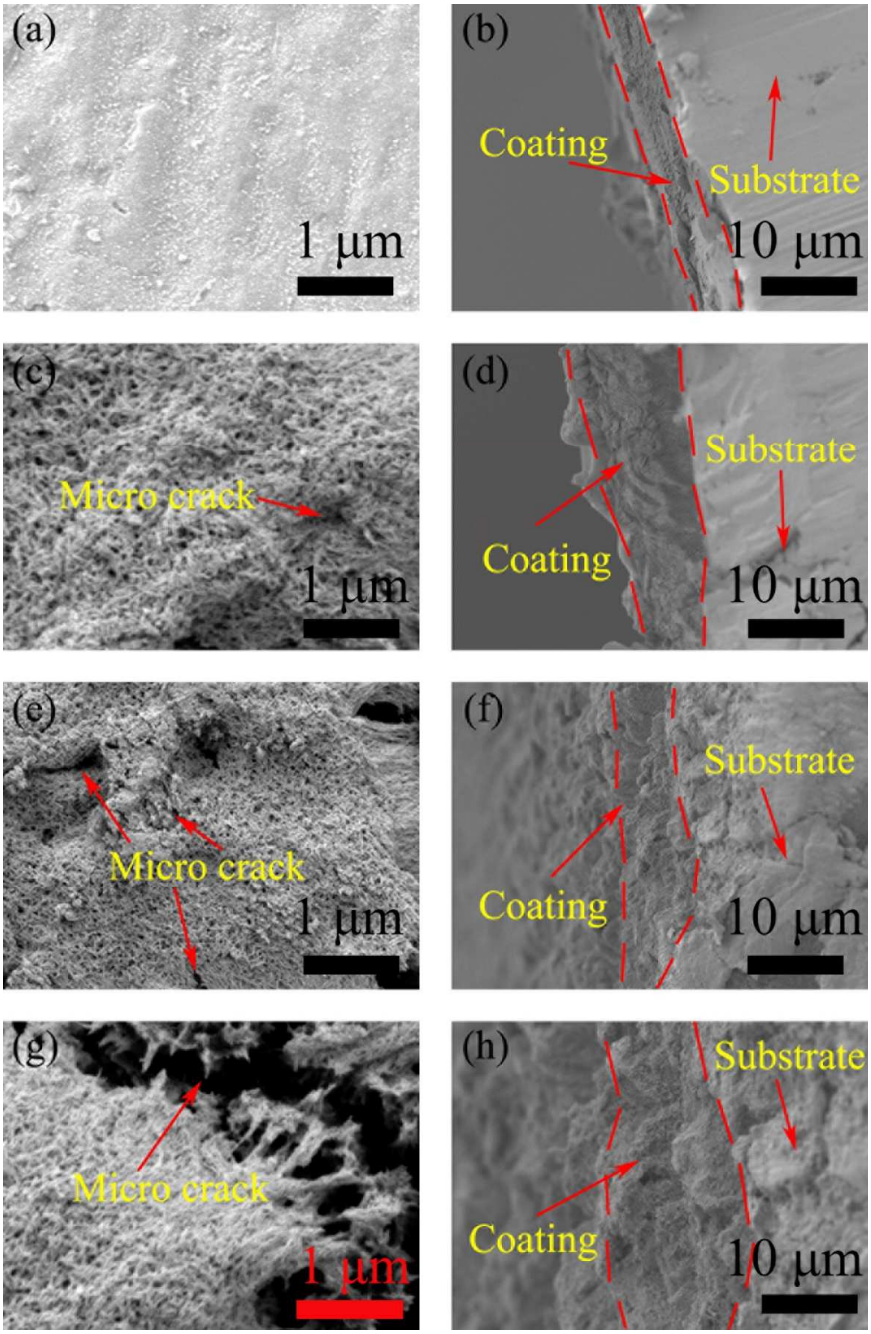

Figure 1. Micro surface and cross-section of Cu_2O/Al_2O_3 coating. (**a**) Micro surface and (**b**) cross-section of Cu_2O/Al_2O_3 coating without heating; (**c**) micro surface; (**d**) cross-section of Cu_2O/Al_2O_3 coating heating at 200 °C; (**e**) micro surface and (**f**) cross-section of Cu_2O/Al_2O_3 coating heating at 300 °C; (**g**) micro surface and (**h**) cross-section of Cu_2O/Al_2O_3 coating heating at 400 °C.

2.2. Elements and Crystalline Structure Analysis of the Cu_2O/Al_2O_3 Coating

Image J software was used to study the distribution of pore sizes on the Cu_2O/Al_2O_3 coating before and after being heated at 300 °C; the results were shown in Figure 2a. It can be seen that when the Cu_2O/Al_2O_3 coating was prepared on the surface of aluminium alloys, there were many through-pores in the coating. Most of the pore diameters were less than 10 nm, and a few were more than 100 nm. After the coating was heated at 300 °C, the ratio of pore sizes less than 10 nm decreased, and that of pore sizes more than 100 nm increased. Although the ratio of mesopores varied slightly, the ratio of the large pore, mesopores, and small pores was more uniform, which was conducive to improving the catalytic performance of the Cu_2O/Al_2O_3 coating in degrading organic compounds and its intermediates. The distribution of Cu, Al, and O was studied by an energy dispersive spectrometer, and the results are displayed in Figure 2b. After electrochemical deposition and heating treatment, Cu_2O was dispersed on the surface or in the pore of anodic coatings uniformly. Even when magnification of the SEM photos was 20,000 times, Cu (I) oxide particles could hardly be seen, indicating that Cu (I) oxide was loaded in the Al_2O_3 coating in the form of nano Cu_2O.

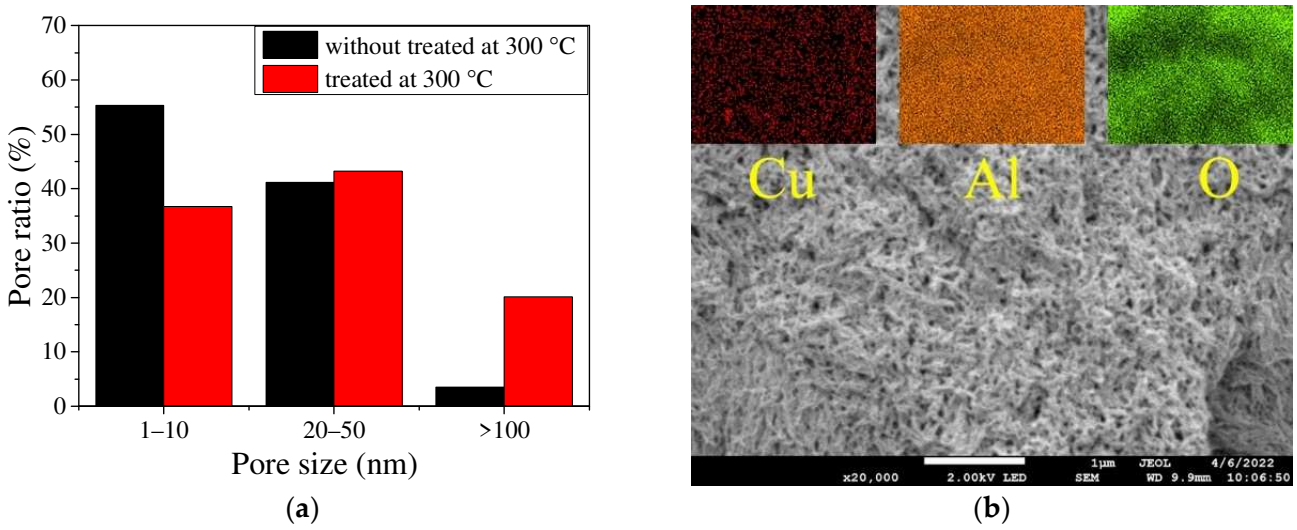

Figure 2. (**a**) Pore size and (**b**) element distribution of Cu_2O/Al_2O_3.

Compared with amorphous Cu (I) oxide, crystalline Cu (I) oxide has better catalytic activity; however, Cu (I) oxide nanoparticles obtained by electrochemical deposition technology are amorphous. To transform amorphous Cu (I) oxide into a crystalline structure, samples were heated at 300 °C with an anodic current density of 50 mA/cm^2, a reaction temperature of 4 °C for 40 min in a 10 wt.% H_2SO_4 solution. Samples were prepared with and without the coating via electrochemical deposition for 30 min, and were heated at 300 °C. Their XRD spectra are shown in Figure 3. Before the Al_2O_3 and Cu_2O/Al_2O_3 coatings were heated at 300 °C, their XRD spectra were smooth curves, illustrating that the coatings were composed of amorphous components. When the coatings were heated at 300 °C, obvious characteristic peaks appeared [44], which proved the amorphous Cu (I) oxide and Al_2O_3 were transformed into crystalline structures. At 44.3°, 45.4° and 66.6°, there were Al_2O_3 characteristic peaks in the XRD spectra of the Al_2O_3 and Cu_2O/Al_2O_3 coatings, while at 38.2°, 77.9° and 85.1°, there were Cu_2O characteristic peaks in the XRD spectra of the Cu_2O/Al_2O_3 coating, but not in the Al_2O_3 coating. This shows that amorphous coatings could be transformed into crystalline Cu_2O/Al_2O_3 coatings by anodizing, electrochemical deposition, and the heating treatment.

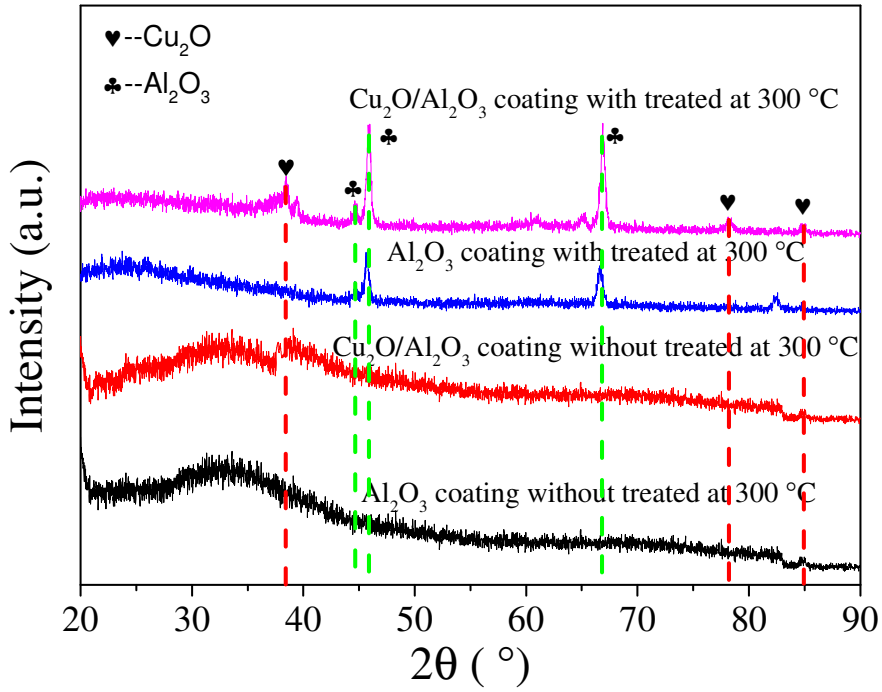

Figure 3. X-ray diffraction (XRD) patterns of Al_2O_3 and Cu_2O/Al_2O_3 coating before and after being treated at 300 °C.

Figure 4 illustrates full and narrow range X-ray photoelectron spectroscopy of Cu_2O/Al_2O_3 coatings prepared with an anodic current density of 50 mA/cm^2, a reaction temperature of 4 °C for 40 min in a 10 wt.% H_2SO_4 solution, and after electrochemical deposition of the coatings and heating at 300 °C. The binding energy values corresponding to the opto-electronic peaks of Cu 2p are 929.66 eV and 949.52 eV [45], respectively. Since the binding energy complies well with the standard value (932.5 eV) of Cu_2O, and the standard value of Cu 2p 3/2 binding energy in different copper oxides, it can be confirmed that the Cu (I) oxide in the Al_2O_3 coating was Cu_2O.

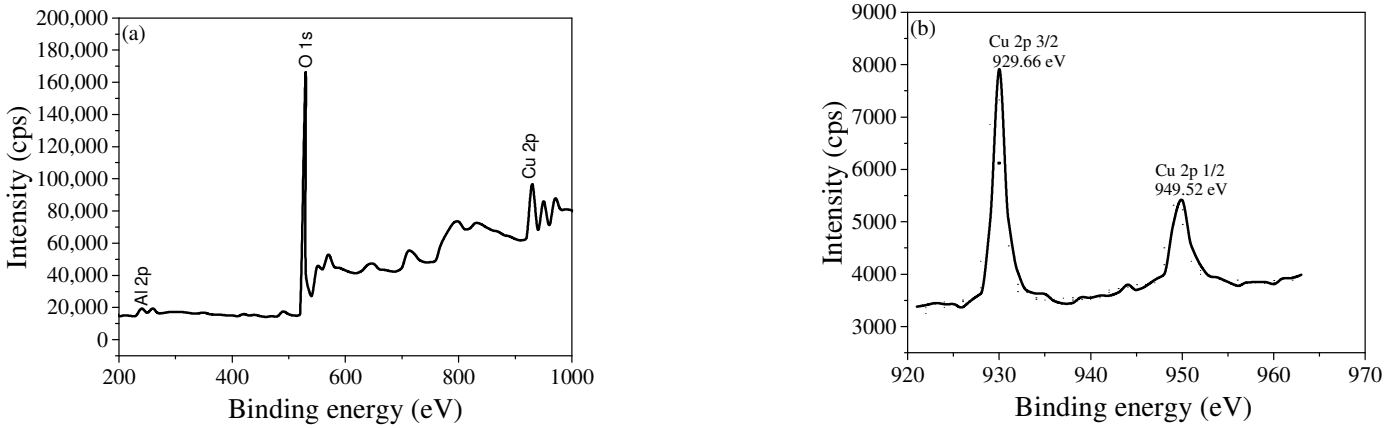

Figure 4. The (**a**) full range and (**b**) narrow range XPS spectrum of the Cu_2O/Al_2O_3 coating.

2.3. Degradation of Methyl Orange Catalyzed by the Cu_2O/Al_2O_3 Coating

The catalytic performances of Cu_2O/Al_2O_3 coatings were studied by assessing degradation of a methyl orange solution at a concentration of 20 mg/L. The effect of process parameters on the degradation of methyl orange is illustrated in Figure 5. It can be seen that without catalyst, methyl orange was not degraded within 180 min. When using the Al_2O_3 coating as a catalyst, the degradation of methyl orange was low within 180 min, whereas the degradation rate of methyl orange increased when using the Cu_2O/Al_2O_3

coating as the catalyst, especially when 3% or 8% H_2O_2 was mixed in the solution and the coating was heated at 300 °C. The results show that the crystalline Cu_2O/Al_2O_3 coating has a good degradation effect on methyl orange in the process of CWPO. Furthermore, using H_2O_2 as an oxidant can increase the degradation rate of methyl orange. However, increasing the H_2O_2 concentration can only accelerate the degradation efficiency, but not improve the degradation rate of methyl orange [46].

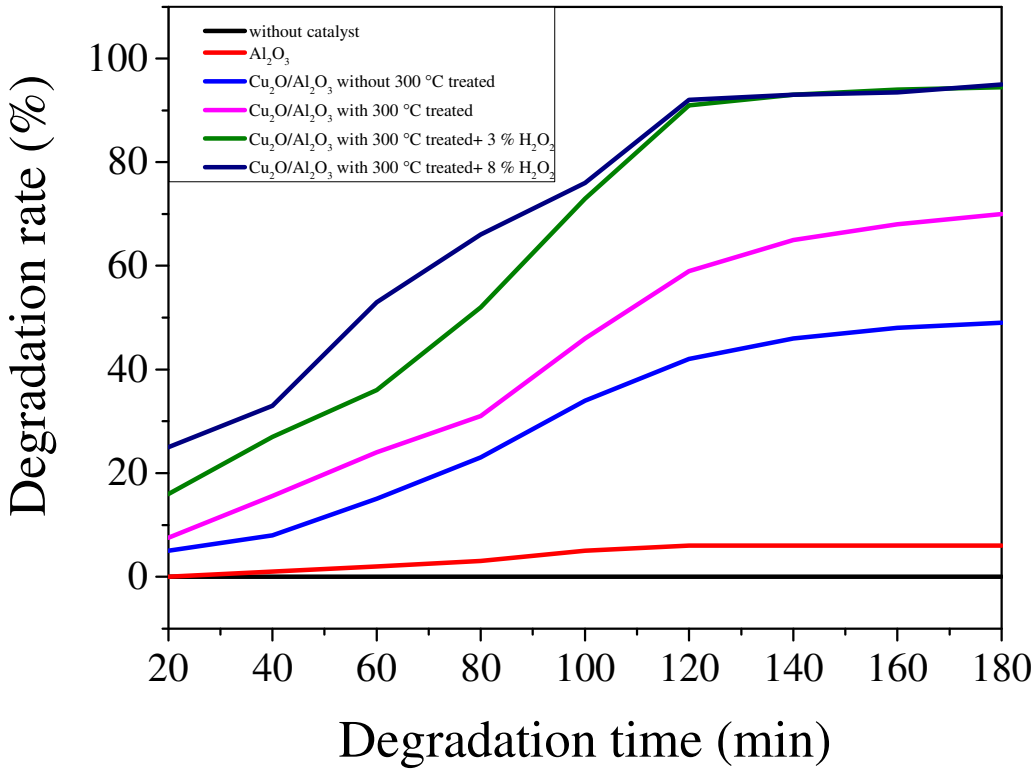

Figure 5. Degradation rate comparison of methyl orange by different coatings.

Based on the above research, using H_2O_2 with a concentration of 3 wt.% as the oxidant, and the Cu_2O/Al_2O_3 coating as the catalyst, methyl orange can be degraded within 120 min. However, the effect of process parameters, such as load mass of Cu (I) oxide, degradation temperature, catalyst dosages, and stability was not clear. To study the suitable degradation condition of methyl orange in the process of CWPO, the influence of the above parameters was investigated, and results are presented in Figure 6. It can be seen from Figure 6a that within 30 min, the absorbance of methyl orange decreased with the increase of electrochemical deposition time. When the electrochemical deposition time increased to 35 min, the absorbance decreased. In addition, it can be seen from Figure 6b that the absorbance of methyl orange at 25 °C was lower than that at 15 °C and 40 °C.

Figure 6c shows that the absorbance of methyl orange decreased with an increased catalyst dosage from 3 to 8 g, and when the catalyst increased to 10 g, the absorbance of methyl orange was maintained. Moreover, Figure 6d illustrates that the absorbance of methyl orange gradually increased with increasing of catalyst reuse times. According to the absorbance of methyl orange solution is linearly related to its concentration. Compared with the initial methyl orange solution, its absorbance decreased by different degrees with different deposition times, catalytic temperature, and catalyst dosage. The smaller the absorbance, the higher the degradation efficiency of the Cu_2O/Al_2O_3 coating. To further study the influence of catalytic condition on the degradation rate of methyl orange, the degradation rate of methyl orange at different conditions was investigated. Results are shown in Figure 7.

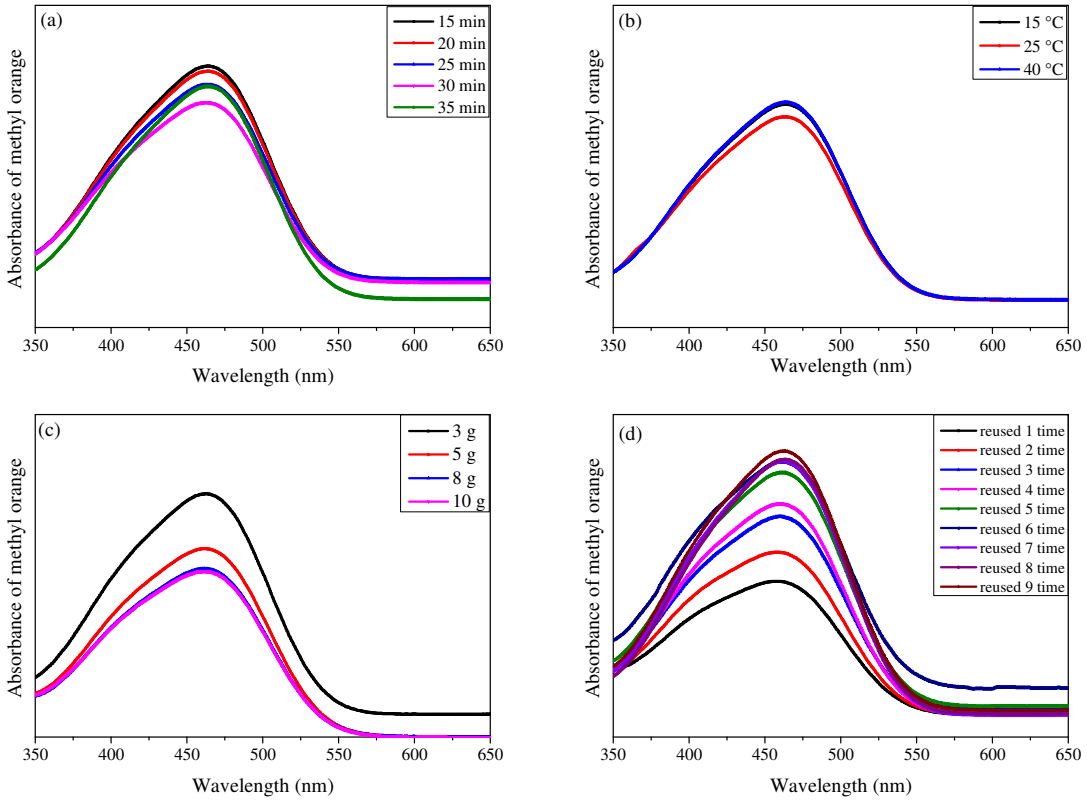

Figure 6. Influence of (**a**) electrochemical deposition time, (**b**) degradation temperature, (**c**) catalyst dosage, and (**d**) reuse times on the absorbance of methyl orange.

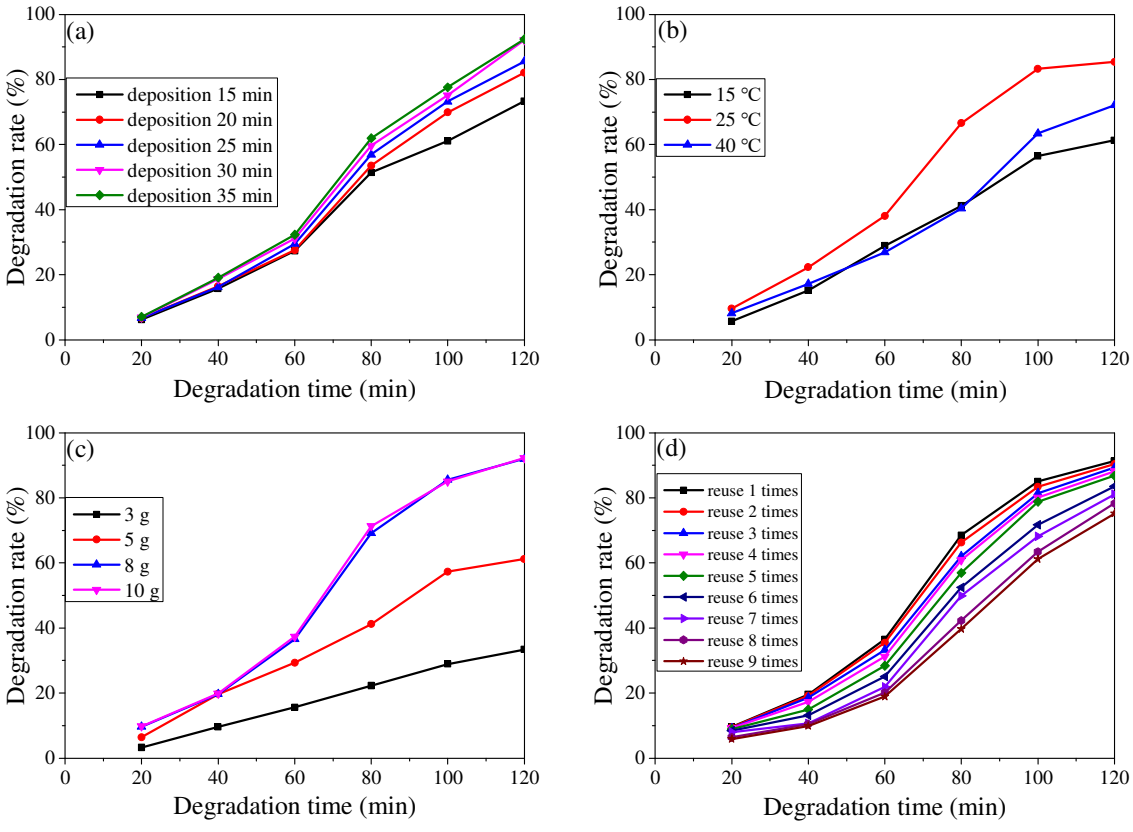

Figure 7. Influence of (**a**) electrochemical deposition time, (**b**) degradation temperature, (**c**) catalyst dosage, and (**d**) reuse times on the degradation rate of methyl orange.

Figure 7a shows that with prolonged treatment time, the degradaton rate of methyl orange increased. When the deposition time of Cu (I) oxide was less than 30 min, the degradation of methyl orange increased, while when the deposition time increased to 35 min, the degradation rate of methyl orange was maintained. The main reason is that the load mass of Cu (I) oxide increased with the increase of deposition time. When the deposition time was short, the catalytic activity of Cu_2O/Al_2O_3 coatings increased with the increase in load mass of Cu (I) oxide. However, in the action of electrochemical deposition, Cu (I) oxide was absorbed not only in the pore but also on the surface of the Al_2O_3 coating. When the deposition was too long, most absorbance was on the surface of the coating, and removed during the subsequent cleaning process. In addition, the micro pores in the Al_2O_3 coating were sealed by Cu (I) oxide, which reduced the active site of the catalyst, and decreased the activity of the Cu_2O/Al_2O_3 coating. It can be seen from Figure 7b that the degradation rate of methyl orange at 25 °C was much higher than at 15 °C and 40 °C, mainly because when the temperature is low, the catalytic activity of the Al_2O_3 coating is low, while when the temperature is high, the decomposition rate of H_2O_2 is too fast, both of which decrease the degradation rate of methyl orange. When the temperature was 25 °C, the rate of ·OH generation was high, and the decomposition rate of H_2O_2 was slow. Thus, the Cu_2O/Al_2O_3 coating had a higher catalytic efficiency at 25 °C. From Figure 7c it can be seen that when the catalyst dosage was 3, 5 and 8 g, the degradation rate of methyl orange was 33.4, 61.2 and 92.0%, respectively. However, when the catalyst dosage increased to 10 g, the degradation rate of methyl orange increased little. The main reason is the catalytic reaction in the CWPO process is not only related to the catalytic activity but also to the adsorption and detachment rate. When the catalyst dosage reached 8 g, the reaction rate was no longer the rate-determining step. Therefore, the methyl orange degradation rate changed insignificantly. Moreover, in Figure 7d, it can be seen that the degradation rate of methyl orange gradually decreased with the increase of catalyst reuse times. After the catalyst was reused 9 times, the degradation rate of methyl orange still reached 75%, which proved the catalyst had good stability. Although the degradation rate of methyl orange was lower than that in the literature, during the CWPO process the degradation efficiency of Cu_2O/Al_2O_3 coating was higher, and the reaction temperature was lower than that in the literature [47,48].

During the CWPO process, the degradation of methyl orange is first-order reaction. In our study, the concentration of H_2O_2 was 3 wt.%, and the initial concentration of methyl orange was20 mg/L; therefore, the kinetic model is [49]:

$$\ln(C_t) = A - kt \cdot \ln(C_t) \quad (1)$$

where C_t represents the concentration of methyl orange at different times, t represents reaction time, and k represents the reaction rate constant. k consists of three parts, namely, Cu_2O electrochemical deposition time (k_1), reaction temperature (k_2), and catalyst dosage (k_3).

According to Formula (1), taking $\ln(C_t)$ and t as straight lines, the slope is the reaction rate constant of methyl orange under different conditions. The degradation rates of methyl orange under different conditions were studied. The linear relation between the logarithm of degradation rate and operation parameters were fitted using Origin 9.1. Results are shown in Figure 8 and Table 2.

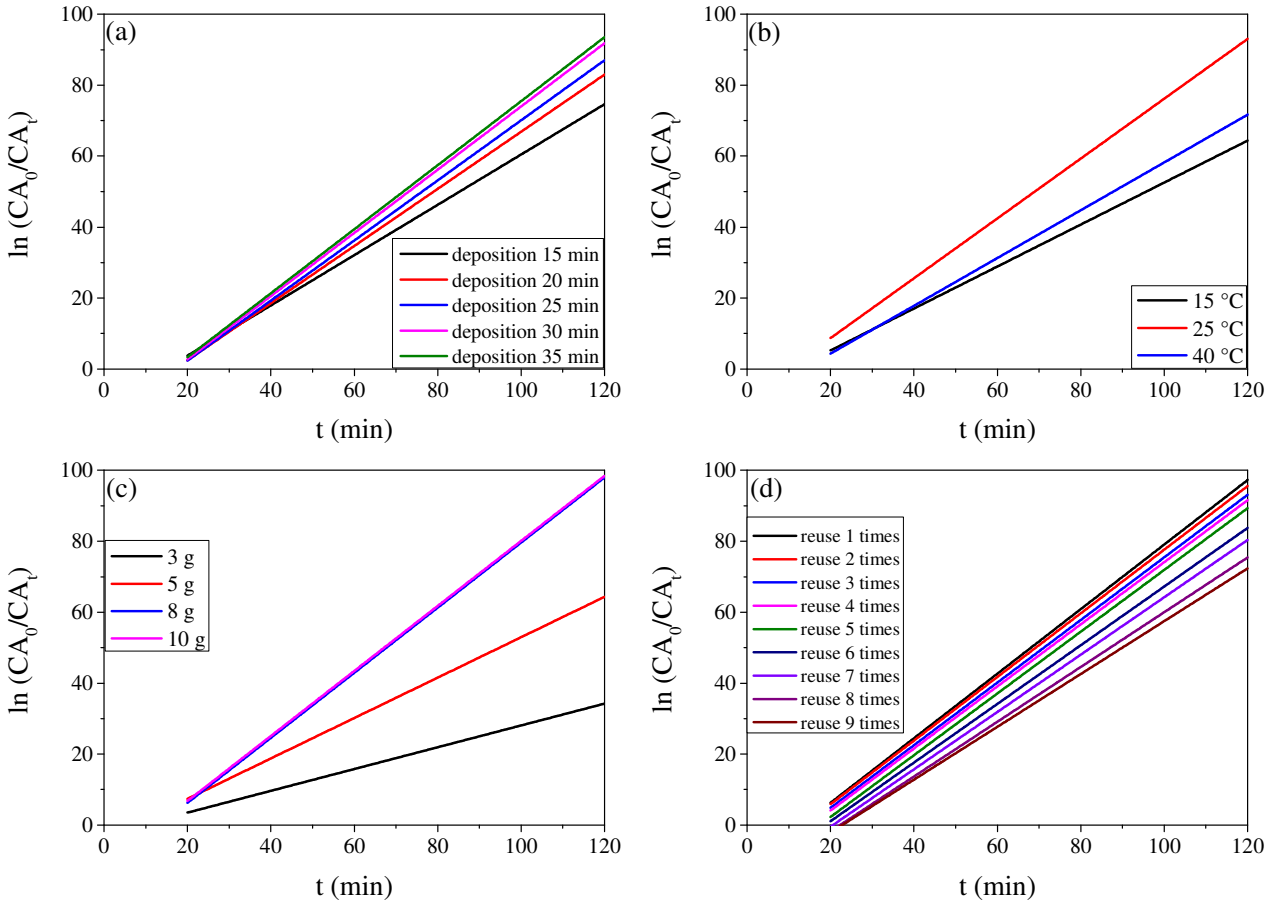

Figure 8. Fitting of methyl orange degradation kinetics model at different (**a**) electrochemical deposition time, (**b**) degradation temperature, (**c**) catalyst dosage, and (**d**) reuse times.

Table 2. Reaction rate equation, reaction rate constant, and variance of methyl orange degradation at different condition.

Reaction Parameters	Value	Reaction Rate Equation	K	R^2
Deposition time (min)	15	Ln (C_t) = −10.45 + 0.71 t	0.71	0.98
	20	Ln (C_t) = −13.65 + 0.81 t	0.81	0.98
	25	Ln (C_t) = −14.61 + 0.85 t	0.85	0.98
	30	Ln (C_t) = −15.11 + 0.89 t	0.89	0.98
	35	Ln (C_t) = −14.75 + 0.90 t	0.90	0.98
Temperature (°C)	15	Ln (C_t) = −6.62 + 0.59 t	0.59	0.99
	25	Ln (C_t) = −8.17 + 0.84 t	0.84	0.95
	40	Ln (C_t) = −9.13 + 0.67 t	0.67	0.97
Catalyst dosage (g)	3	Ln (C_t) = −2.66 + 0.31 t	0.31	1.00
	5	Ln (C_t) = −4.02 + 0.57 t	0.57	0.98
	8	Ln (C_t) = −12.12 + 0.92 t	0.92	0.96
	10	Ln (C_t) = −11.56 + 0.92 t	0.92	0.95
Reuse times	1	Ln (C_t) = −11.93 + 0.91 t	0.91	0.96
	2	Ln (C_t) = −12.07 + 0.90 t	0.90	0.96
	3	Ln (C_t) = −12.79 + 0.88 t	0.88	0.97
	4	Ln (C_t) = −13.43 + 0.88 t	0.88	0.96
	5	Ln (C_t) = −15.14 + 0.87 t	0.87	0.95
	6	Ln (C_t) = −15.47 + 0.83 t	0.83	0.96
	7	Ln (C_t) = −16.64 + 0.81 t	0.81	0.94
	8	Ln (C_t) = −17.21 + 0.77 t	0.77	0.95
	9	Ln (C_t) = −16.99 + 0.74 t	0.74	0.94

It can be seen that with the prolongation of deposition time, the reaction rate constant increased from 0.71 to 0.90, but when the deposition time reached 30 min, the degradation rate constant reached 0.89, showing that methyl orange could be rapidly degraded when the deposition was 30 min. The degradation rate constant of methyl orange at 25 °C was 0.84, while when reaction temperatures were 15 °C and 40 °C, the degradation rate constant were 0.59 and 0.67, respectively. This shows the degradation rate of methyl orange at 25 °C was the fastest. With increases of catalyst dosage from 3 g to 10 g, the degradation rate constant of methyl orange increased from 0.31 to 0.92, but when the catalyst dosage reached 8 g, the constant reached 0.92, indicating that further increasing the catalyst dosage could not accelerate the degradation rate of methyl orange. With increased reuse times, the degradation rate constant decreased slowly. When the reuse reached 9 times, the degradation rate constant was 0.74, and the catalyst still had high degradation efficiency, proving that the Cu_2O/Al_2O_3 coating has excellent stability during CPWO process.

To further study why the degradation rate of methyl orange decreases with increased reuse times, scanning electron microscopy was used to investigate the micro surface structure and crystalline structure of the coating. Results ae showed in Figures 9 and 10. It can be seen from Figure 9 that with the increase of reuse times, the size and quantity of the micro cracks in the Cu_2O/Al_2O_3 coating increased, and big pores appeared in the coating. It is well known that the catalytic activity of the coating decreases with decreasing surface area; therefore, the degradation rate of methyl orange decreased with the increase of the coating's reuse time. It also can be seen that the pore size of the coating decreased first and then increased with increasing reuse time. The probable reason is that methyl orange can be absorbed on the surface of the coating. After the catalyst was immersed in methyl orange solution, methyl orange was deposited on the surface of the coating, which decreased the pore size. With the further increase of reuse time, the methyl orange promoted the recrystallization of Cu_2O in the coating. Therefore, the pore size of the Cu_2O/Al_2O_3 coating increased.

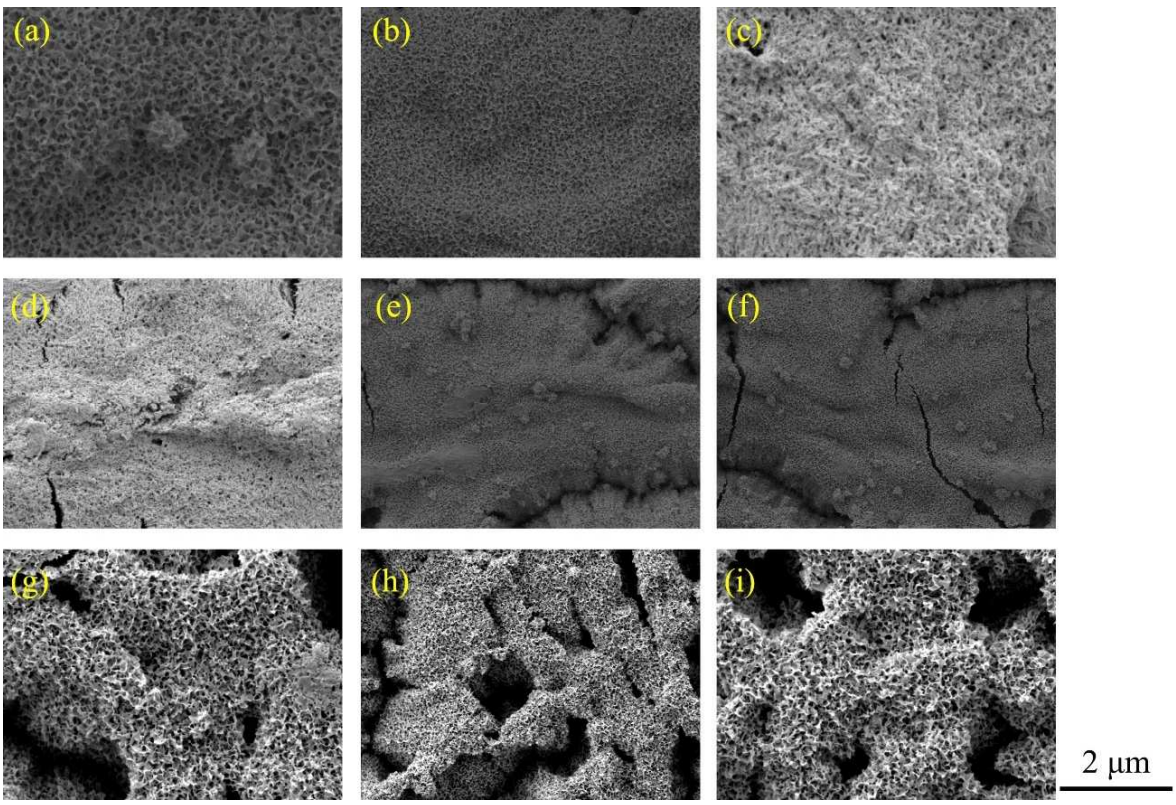

Figure 9. Micro surface photograph of the Cu_2O/Al_2O_3 coating after being reused (**a**) once, (**b**) twice, (**c**) 3 times, (**d**) 4 times, (**e**) 5 times, (**f**) 6 times, (**g**) 7 times, (**h**) 8 times and (**i**) 9 times.

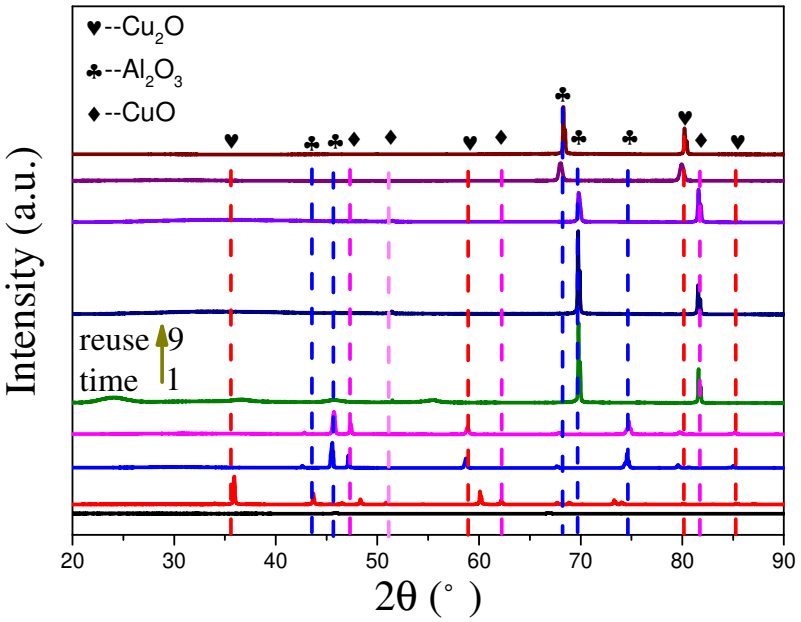

Figure 10. X-ray diffraction (XRD) patterns of Cu_2O/Al_2O_3 coating after nine reuse times.

An X-ray diffractometer was used to study the crystalline structure of the Cu_2O/Al_2O_3 coating at different reuse times. Results are shown in Figure 10. It can be seen from Figure 11 that at about 36°, 58°, 80° and 85°, there are Cu (I) oxide characteristic peaks, at about 42°, 45°, 68° 70° and 75° there are Al_2O_3 characteristic peaks, and at about 47°, 52°, 62° and 82°, there are Cu (II) oxide characteristic peaks. It can be seen from Figure 9a–i that with the increase of reuse times, the peak intensity of Cu (II) oxide increases, while the peak intensity of Cu (I) oxide decreases, showing that some Cu (I) oxide in the coating is transformed into Cu (II) oxide. The main reason is the Cu (I) oxide in the coating is a metastable oxide. During the process of CPWO, with the action of H_2O_2 some Cu (I) oxide is transformed into Cu (II) oxide. Because Cu (I) oxide is the active species for degradation of methyl orange, the catalytic activity of the Cu_2O/Al_2O_3 coating decreases with the decrease of Cu (I) oxide. Therefore, the degradation rate of methyl orange decreases with increasing reuse times.

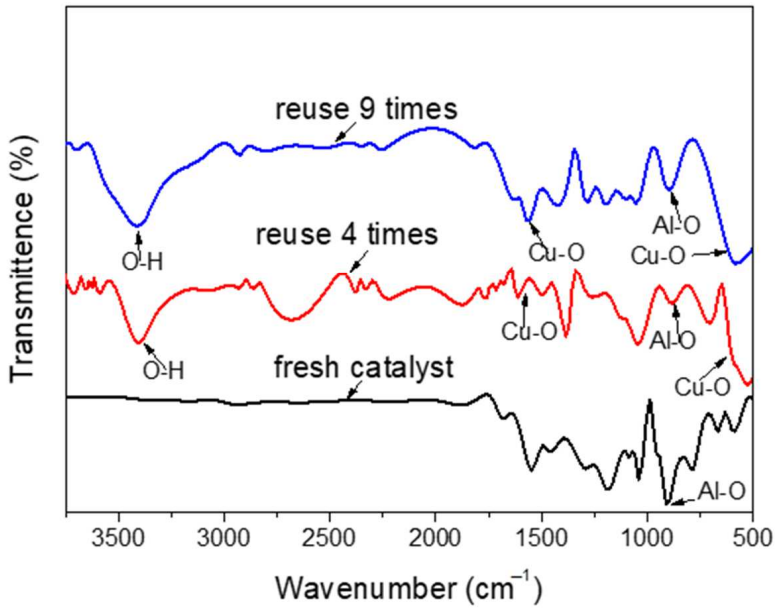

Figure 11. FT-IR spectrum of Cu_2O/Al_2O_3 coating after reuse 0, 4, and 9 times.

With the increase of reuse times, a wide peak appeared in the range of 20–30°. The possible reason is that some alumina or Cu (I/II) oxide in the coating combined with water to form an amorphous product, which also led to decrease of catalyst activity. Figure 11 shows the infrared absorption peaks of Cu_2O/Al_2O_3 coatings after catalyst reuse 0, 4, and 9 times. The peaks at 3406 cm^{-1} can be assigned to the O-H stretching vibrations, the peaks at 1630 cm^{-1}, 648 cm^{-1} correspond to Cu-O stretching vibrations [50] and the peaks at 838 cm^{-1} can be assigned to Al-O stretching vibrations [51]. It can be seen that with increasing reuse times, the characteristic peak intensity of O-H increased, but the peak intensity of Al-O decreased, while the peak intensity of was Cu-O maintained. The FTIR spectra showed that crystalline Al_2O_3 or Cu (I) oxide combined with H_2O formed amorphous products.

The degradation of methyl orange by other catalysts reported in the literature were compared with our current study and are shown in Table 3. It can be seen that the degradation efficiency of the Cu_2O/Al_2O_3 coating is close to that of nanoparticle catalysts reported in the literature, while the reuse time can reach 9 times, and does not require other auxiliary measures such as light energy. Thus, the degradation process of methyl orange can be simplified.

Table 3. Comparison of degradation efficiency of Cu_2O/Al_2O_3 coating with other catalysts reported in the literature.

Catalyst	Reaction Condition	Degradation Efficiency	Reference
Cu_2O	Dye concentration: 10 mg/L	94.54% in 4 h	[52]
CuO/ZnO	Dye concentration: 5 ppm pH 6.8, Catalyst dosage: 0.6 g Light source: UV-light	54.1% in 4 h	[53]
CuO/NC NPs	Dye concentration: 30 ppm Catalyst dosage: 0.015 g Light source: UV and visible	97.18% in 4 min (UV) 95.96% in 4 min (Vis)	[54]
SiNWs–CuNPs	Dye concentration: 20 ppm Dye amount: 20 mL Light source: visible (5 LEDS)	89% in 120 min	[3]
Cu_2O/Al_2O_3	Dye concentration: 20 mg/L Catalyst dosage: 8 g H_2O_2 concentration: 3 wt.%	92% in 120 min	Current study

3. Experiment

3.1. Experimental Materials

Each of the experimental reagents was provided by Tianjin Kemiou Chemical Reagent Co. Ltd. (Tianjin, China), and commercial aluminium alloy 1060 (20 × 20 × 1 mm^3) was used as a specimen.

3.2. Experimental Process

3.2.1. Preparation of Cu_2O/Al_2O_3 Coating

Using a DC supply, aluminium alloys were used as anodes and stainless steel was used as the cathode, respectively. The anodizing procedure was conducted with a stirring speed of 60 rpm and a current density of 50 mA/cm^2 at 4 °C for 40 min in a 10 wt.% H_2SO_4 solution. Coatings were subjected to an anodizing treatment as cathodes, and a copper plate was used as the anode. Electrochemical deposition Cu (I) oxide on the surface of the coating lasted for 30 min. Finally, the Cu_2O/Al_2O_3 coating was heated at 300 °C for 2 h.

3.2.2. Degradation of Methyl Orange

Methyl orange powder has a maximum absorbance at 460 nm (Figure 12a), which changes with its concentration linearly (seen in Figure 12b). A volume of 200 mL of methyl orange with a concentration of 20 mg/L was used to simulate dye wastewater, and the degradation of methyl orange was produced in a heated magnetic stirrer reactor

at atmospheric pressure and 25 ± 1 °C for 3 h. Then, 2 mL methyl orange was removed from the original solution, and the degradation rate of methyl orange was determined by measuring its absorbance at 460 nm using a 723 N UV-Visible spectrophotometer.

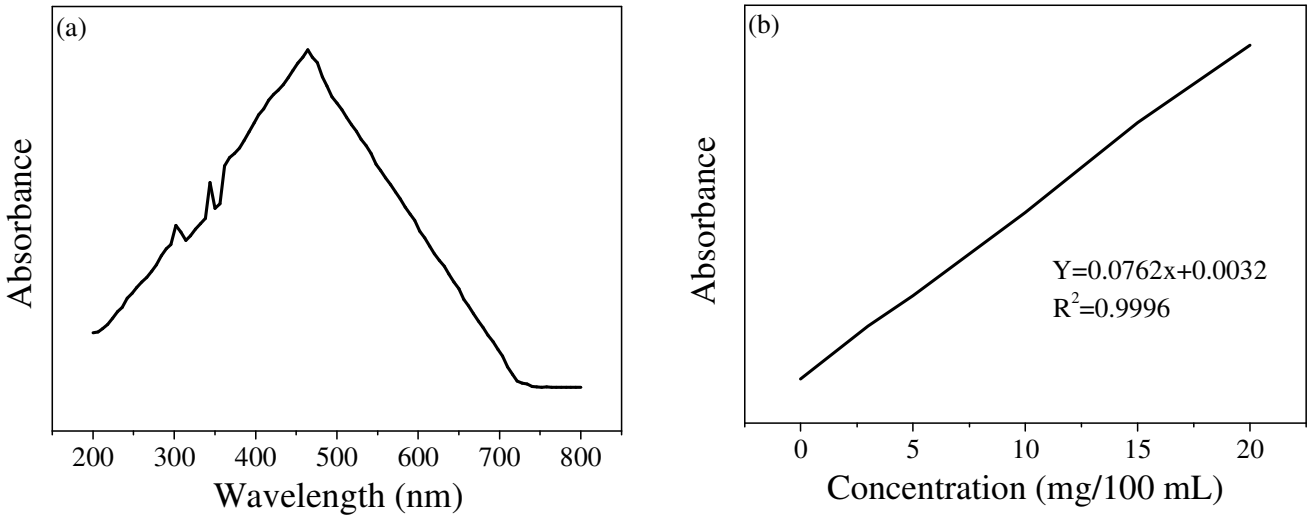

Figure 12. UV-Vis spectra of methyl orange at different (**a**) wavelengths and (**b**) concentrations.

3.3. Characteristics

The radiation emitted by the sample surface was detected by a Fourier transform infrared (FT-IR) spectrometer (JASCO FT/IR-6100). An X-ray diffractometer (XRD, (D/max-rB, RICOH, Tokyo, Japan) with CuKa sources was employed to examine the phase compositions for diverse coatings. The current applied and accelerating voltage were 30 mA and 40 kV, respectively. Scanning electron microscopy (SEM, S-4700, Hitachi, Tokyo, Japan) was used to investigate the cross-section and surface microstructures of the coating, while the porosity of the coatings was statistically analyzed by Image J software. An energy dispersive spectrometer was used for quantitative and qualitative analysis of element points, lines, and surfaces. The resolution of the secondary electron image of SEM was less than 3.0 nm, with an element detection range of Be(4)–Am(95). An AXIS-ULTRA X-ray photoelectron spectroscopy (XPS) was used to analyze the film. The analysis involved a Ka line of Al (150 W, 15 kV, 1486.6 eV), a vacuum degree of 10^{-9} Torr, and the carbon peak (284.8 eV) of the hydrocarbons on the surface of the standard sample. Before the test, Ar^+ ions were used to bombard the inner cavity to remove the contamination layer on the sample surface. In addition, DR 5000 UV-vis spectroscopy was conducted to determine the absorbance of Cu_2O/Al_2O_3 at different wavelength ranges. A 723 N UV-vis spectroscopy was used to test and compare the absorbance of methyl orange solution at 464 nm wavelength before and after photocatalysis treatment. Then, the degradation rate of the sample under room temperature and normal pressure conditions could be obtained. Scans were performed in the range of 200 to 800 nm at the scan rate of 1 nm/s^{-1}. Formula (2) was used to determine absorbance before and after the photocatalytic treatment [55].

$$A = \lg(I_t/I_0) \quad (2)$$

In Formula (10), A is absorbance, I_t is transmitted light intensity, and I_0 is the incident light intensity. According to Formula (2), the catalytic activity of Cu_2O/Al_2O_3 can be determined by the degradation rate of methyl orange.

$$\eta = \frac{(C_0 - C_t)}{C_0} \times 100\% = \frac{(A_0 - A_t)}{A_0} \times 100\% \quad (3)$$

In Formula (3), η refers to the degradation rate of methyl orange (%), C_0 and C_t represent methyl orange concentration (mg/L) before and after photocatalytic degradation, respectively, and A_0 and A_t are the absorbances of methyl orange before and after treatment.

4. Conclusions

A Al_2O_3 coating was prepared on the surface of aluminium alloys by an anodizing technology with a current density of 50 mA/cm^2 at 4 °C for 40 min in a 10 wt.% H_2SO_4 solution. Then, Cu (I) oxide particles were deposited electrochemically in the coating for 30 min.

The microstructure and crystalline structure of the coating was studied by SEM, XRD, EDS, and XPS, and results showed that the crystalline Cu (I) oxide was evenly dispersed in the pore and on the surface of the Al_2O_3 coating.

Suitable catalytic conditions were studied by measuring the absorbance of methyl orange, and results showed that the degradation rate of methyl orange could reach 92% when the electrochemical deposition time was 30 min, with a catalyst dosage of 8 g and a temperature of 25 °C for 120 min. The degradation rate was 75% after the catalyst was reused 9 times. The catalytic efficiency and condition of the catalyst was improved. Compared with similar catalysts reported in the literature, the Cu_2O/Al_2O_3 coating has a similar degradation efficiency and higher stability. In addition, the degradation process of methyl orange can be simplified.

Author Contributions: Conceptualization, P.Z. and D.-b.L.; methodology, D.-b.L.; software, P.Z.; validation, P.Z. and D.-b.L.; formal analysis, P.Z.; investigation, D.-b.L.; resources, P.Z.; data curation, P.Z.; writing—original draft preparation, P.Z.; writing—review and editing, D.-b.L. and J.W.; visualization, P.Z. and J.W.; supervision, P.Z.; project administration, D.-b.L. and J.W.; funding acquisition, D.-b.L. All authors have read and agreed to the published version of the manuscript.

Funding: This research was funded by Zhengzhou Key Laboratory of Fiber Reinforced Polymer Composites (Grant No. 02032146) and Science and Technology Research Project of Henan Provincial Department of Science and Technology (Grant No. 212102210249).

Data Availability Statement: The data that support the findings of this study are available on request from the corresponding author.

Conflicts of Interest: The authors declare no conflict of interest to this work.

References

1. Saratale, R.; Saratale, G.; Chang, J.; Govindwar, S. Bacterial decolorization and degradation of azo dyes: A review. *J. Taiwan Inst. Chem. Eng.* **2011**, *42*, 138–157. [CrossRef]
2. Chen, C.Y.; Chen, J.N.; Chen, S.D. Toxicity assessment of industrial wastewater by microbial testing method. *Water Sci. Technol.* **1999**, *39*, 139–143. [CrossRef]
3. Khan, I.; Khan, I.; Usman, M.; Imran, M.; Saeed, K. Nanoclay-mediated photocatalytic activity enhancement of copper oxide nanoparticles for enhanced methyl orange photodegradation. *J. Mater. Sci. Mater. Electron.* **2020**, *31*, 8971–8985. [CrossRef]
4. Tauber, M.M.; Guebitz, G.M.; Rehorek, A. Degradation of Azo Dyes by Laccase and Ultrasound Treatment. *Appl. Environ. Microbiol.* **2005**, *71*, 2600–2607. [CrossRef] [PubMed]
5. Chen, Z.; Li, D.; Zhang, W.; Shao, Y.; Chen, T.; Sun, M.; Fu, X. Photocatalytic degradation of dyes by $ZnIn_2S_4$ microspheres under visible light irradiation. *J. Phys. Chem. C* **2009**, *113*, 4433–4440. [CrossRef]
6. Uri, K.I.; Ostafe, R.; Prodanovi, O.; Delmas, A.; Popovic, N.; Fischer, R.; Schillberg, S.; Prodanociv, R. Improved degradation of azo dyes by lignin peroxidase following mutagenesis at two sites near the catalytic pocket and the application of peroxidase-coated yeast cell walls. *Front. Environ. Sci. Eng.* **2021**, *15*, 1–10.
7. Ain, Q.U.; Rasheed, U.; Yaseen, M.; Zhang, H.; Tong, Z. Superior dye degradation and adsorption capability of polydopamine modified Fe_3O_4-pillared bentonite composite. *J. Hazard. Mater.* **2020**, *397*, 122758. [CrossRef]
8. Kang, Y.-G.; Yoon, H.; Lee, C.-S.; Kim, E.-J.; Chang, Y.-S. Advanced oxidation and adsorptive bubble separation of dyes using MnO_2-coated Fe_3O_4 nanocomposite. *Water Res.* **2019**, *151*, 413–422. [CrossRef]
9. Rendon, S.M.K.; Mavrynsky, D.; Meierjohann, A.; Tiihonen, A.; Miettunen, K.; Asghar, M.I.; Halme, J.; Kronberg, L.; Leino, R. Analysis of dye degradation products and assessment of the dye purity in dye-sensitized solar cells. *Rapid Commun. Mass Spectrom.* **2015**, *29*, 2245–2251. [CrossRef]

10. Zhu, G.; Fang, H.; Xiao, Y.; Hursthouse, A.S. The Application of Fluorescence Spectroscopy for the Investigation of Dye Degradation by Chemical Oxidation. *J. Fluoresc.* **2020**, *30*, 1271–1279. [CrossRef]
11. Syafalni; Lim, H.K.; Ismail, N.; Abustan, I.; Murshed, M.F.; Ahmad, A. Treatment of landfill leachate by using lateritic soil as a natural coagulant. *J. Environ. Manag.* **2012**, *112*, 353–359. [CrossRef] [PubMed]
12. Ovejero, G.; Sotelo, J.L.; Rodríguez, A.; Vallet, A.; Garcia, J. Wet air oxidation and catalytic wet air oxidation for dyes degradation. *Environ. Sci. Pollut. Res.* **2011**, *18*, 1518–1526. [CrossRef] [PubMed]
13. Wang, X.-Q.; Han, S.-F.; Zhang, Q.-W.; Zhang, N.; Zhao, D.-D. Photocatalytic oxidation degradation mechanism study of methylene blue dye waste water with GR/iTO$_2$. *MATEC Web Conf.* **2018**, *238*, 03006. [CrossRef]
14. Varjani, S.; Rakholiya, P.; Ng, H.Y.; You, S.; Teixeira, J.A. Microbial degradation of dyes: An overview. *Bioresour. Technol.* **2020**, *314*, 123728. [CrossRef] [PubMed]
15. Khan, I.; Saeed, K.; Ali, N.; Khan, I.; Zhang, B.; Sadiq, M. Heterogeneous photodegradation of industrial dyes: An insight to different mechanisms and rate affecting parameters. *J. Environ. Chem. Eng.* **2020**, *8*, 104364. [CrossRef]
16. Yang, Y.C.; Lu, Y.G.; Ye, Z.X.; He, L.P.; Yu, J. Phenol Degradation by Catalytic Wet Hydrogen Peroxide Oxidation on Fe/Active Carbon Catalyst. *Adv. Mater. Res.* **2012**, *433–440*, 147–152. [CrossRef]
17. Abhilash, M.R.; Akshatha, G.; Srikantaswamy, S. Photocatalytic dye degradation and biological activities of the Fe_2O_3/Cu_2O nanocomposite. *RSC Adv.* **2019**, *9*, 8557. [CrossRef]
18. Liou, R.-M.; Chen, S.-H.; Hung, M.-Y.; Hsu, C.-S.; Lai, J.-Y. Fe (III) supported on resin as effective catalyst for the heterogeneous oxidation of phenol in aqueous solution. *Chemosphere* **2005**, *59*, 117–125. [CrossRef]
19. Sreeja, P.; Sosamony, K. A Comparative Study of Homogeneous and Heterogeneous Photo-fenton Process for Textile Wastewater Treatment. *Procedia Technol.* **2016**, *24*, 217–223. [CrossRef]
20. Sun, L.; Wang, G.; Hao, R.; Han, D.; Cao, S. Solvothermal fabrication and enhanced visible light photocatalytic activity of Cu_2O-reduced graphene oxide composite microspheres for photodegradation of Rhodamine B. *Appl. Surf. Sci.* **2015**, *358*, 91–99. [CrossRef]
21. Hsueh, C.; Huang, Y.; Wang, C.; Chen, C. Degradation of azo dyes using low iron concentration of Fenton and Fenton-like system. *Chemosphere* **2005**, *58*, 1409–1414. [CrossRef] [PubMed]
22. Catrinescu, C.; Arsene, D.; Dragoi, B.; Teodosiu, C. Catalytic Wet Hydrogen Peroxide Oxidation of 4-Chlorophenol over Iron-Exchanged Clays. *Environ. Eng. Manag. J.* **2010**, *9*, 7–16. [CrossRef]
23. Pariente, M.I.; Melero, J.A.; Martínez, F.; Bottas, A.; Gallego, I. Catalytic wet hydrogen peroxide oxidation of a petrochemical wastewater. *Water Sci. Technol. J. Int. Assoc. Water Pollut. Res.* **2010**, *61*, 1829–1836. [CrossRef] [PubMed]
24. Saeed, K.; Sadiq, M.; Khan, I.; Ullah, S.; Ali, N.; Khan, A. Synthesis, characterization, and photocatalytic application of Pd/ZrO2 and Pt/ZrO_2. *Appl. Water Sci.* **2018**, *8*, 60. [CrossRef]
25. Jalil, E.H.B.; Rahman, S.A.; Zainol, N.; Ajit, A.; Yee, C. Sulfide removal from petrochemical wastewater using catalytic wet air oxidation (CWAO) method ScienceDirect. *Mater. Today Proc.* **2018**, *5*, 22043–22049. [CrossRef]
26. Sengupta, M.; Das, S.; Bordoloi, A. Cu/Cu $_2$ O nanoparticle interface: Rational designing of a heterogeneous catalyst system for selective hydroamination. *Mol. Catal.* **2017**, *440*, 57–65. [CrossRef]
27. Kim, S.-K.; Ihm, S.-K. Nature of carbonaceous deposits on the alumina supported transition metal oxide catalysts in the wet air oxidation of phenol. *Top. Catal.* **2005**, *33*, 171–179. [CrossRef]
28. Lai, C.; He, T.; Li, X.; Chen, F.; Yue, L.; Hou, Z. Catalytic wet air oxidation of phenols over porous plate Cu-based catalysts. *Appl. Clay Sci.* **2019**, *181*, 105253. [CrossRef]
29. Gaudin, P.; Fioux, P.; Dorge, S.; Nouali, H.; Vierling, M.; Fiani, E.; Molière, M.; Brilhac, J.-F.; Patarin, J. Formation and role of Cu+ species on highly dispersed CuO/SBA-15 mesoporous materials for SOx removal: An XPS study. *Fuel Process. Technol.* **2016**, *153*, 129–136. [CrossRef]
30. Wang, H.; Xu, R.; Jin, Y.; Zhang, R. Zeolite structure effects on Cu active center, SCR performance and stability of Cu-zeolite catalysts. *Catal. Today* **2019**, *327*, 295–307. [CrossRef]
31. Sriprom, P.; Neramittagapong, S.; Lin, C.; Wantala, K.; Neramittagapong, A.; Grisdanurak, N. Optimizing chemical oxygen demand removal from synthesized wastewater containing lignin by catalytic wet-air oxidation over CuO/Al_2O_3 catalysts. *J. Air Waste Manag. Assoc.* **2015**, *65*, 828–836. [CrossRef] [PubMed]
32. Taran, O.; Ayusheev, A.B.; Ogorodnikova, O.L.; Prosvirin, I.; Isupova, L.A.; Parmon, V.N. Perovskite-like catalysts $LaBO_3$ (B = Cu, Fe, Mn, Co, Ni) for wet peroxide oxidation of phenol. *Appl. Catal. B Environ.* **2016**, *180*, 86–93. [CrossRef]
33. Sushma; Kumari, M.; Saroha, A.K. Performance of various catalysts on treatment of refractory pollutants in industrial wastewater by catalytic wet air oxidation: A review. *J. Environ. Manag.* **2018**, *228*, 169–188. [CrossRef]
34. Zhao, M.; Shi, J.; Hou, Z. Selective hydrogenation of phenol to cyclohexanone in water over Pd catalysts supported on Amberlyst-45. *Chin. J. Catal.* **2016**, *37*, 234–239. [CrossRef]
35. Zhang, Z.; Chen, C.; Yang, Y.; Zhang, H.; Kim, D.; Sugahara, T.; Nagao, S.; Suganuma, K. Low-temperature and pressureless sinter joining of Cu with micron/submicron Ag particle paste in air. *J. Alloys Compd.* **2018**, *780*, 435–442. [CrossRef]
36. Armaroli, T.; Minoux, D.; Gautier, S.; Euzen, P. A DRIFTS study of Mo/alumina interaction: From Mo/boehmite solution to Mo/γAl2O3 support. *Appl. Catal. A Gen.* **2003**, *251*, 241–253. [CrossRef]
37. Park, B.; Saito, M.; Mizuno, J.; Nishikawa, H. Robust shear strength of Cu–Au joint on Au surface-finished Cu disks by solid-state nanoporous Cu bonding. *Microelectron. Eng.* **2022**, *260*, 111807. [CrossRef]

38. Fukuda, R.; Sakai, S.; Takagi, N.; Matsui, M.; Ehara, M.; Hosokawa, S.; Tanaka, T.; Sakaki, S. Mechanism of NO–CO reaction over highly dispersed cuprous oxide on γ-alumina catalyst using a metal–support interfacial site in the presence of oxygen: Similarities to and differences from biological systems. *Catal. Sci. Technol.* **2018**, *8*, 3833–3845. [CrossRef]
39. Zhang, Y.; Zhou, Y.; Peng, C.; Shi, J.; Wang, Q.; He, L.; Shi, L. Enhanced activity and stability of copper oxide/γ-alumina catalyst in catalytic wet-air oxidation: Critical roles of cerium incorporation. *Appl. Surf. Sci.* **2018**, *436*, 981–988. [CrossRef]
40. Cuauhtémoc, I.; Del Angel, G.; Torres, G.; Angeles-Chavez, C.; Navarrete, J.; Padilla, J. Enhancement of catalytic wet air oxidation of tert-amyl methyl ether by the addition of Sn and CeO_2 to Rh/Al_2O_3 catalysts. *Catal. Today* **2011**, *166*, 180–187. [CrossRef]
41. Abedini, S.; Parvin, N.; Ashtari, P. Preparation, characterization and microstructural optimization of a thin γ-alumina membrane on a porous stainless steel substrate. *Mater. Sci. Eng. A* **2012**, *533*, 1–8. [CrossRef]
42. Rambabu, G.; Naik, D.B.; Rao, C.V.; Rao, K.S.; Reddy, G.M. Optimization of friction stir welding parameters for improved corrosion resistance of AA2219 aluminum alloy joints. *Def. Technol.* **2015**, *8*, 330–337. [CrossRef]
43. Kang, H.; Seungkyu, S.; Yoon, S. A numerical study on the light-weight design of PTC heater for an electric vehicle heating system. *Energies* **2018**, *11*, 1276. [CrossRef]
44. Andrievsky, G.; Klochkov, V.; Bordyuh, A.; Dovbeshko, G. Comparative analysis of two aqueous-colloidal solutions of C60 fullerene with help of FTIR reflectance and UV–Vis spectroscopy. *Chem. Phys. Lett.* **2002**, *364*, 8–17. [CrossRef]
45. Thakur, S.; Gogate, P.R. Synthesis of Pd/C catalyst using formaldehyde reduction method and application for ultrasound assisted transfer hydrogenation of corn oil. *Chem. Eng. Process. Intensif.* **2020**, *152*, 107939. [CrossRef]
46. Vasquez, R.P. Cu_2O by XPS. *Surf. Sci. Spectra* **1998**, *5*, 257–261. [CrossRef]
47. Sotelo, J.L.; Ovejero, G.; Martínez, F.; Melero, J.; Milieni, A. Catalytic wet peroxide oxidation of phenolic solutions over a $LaTi1-xCu_xO_3$ perovskite catalyst. *Appl. Catal. B Environ.* **2004**, *47*, 281–294. [CrossRef]
48. Liu, D.; Jiang, B.; Liu, Z.; Ge, Y.; Wang, Y. Preparation and catalytic properties of Cu_2O–CoO/Al_2O_3 composite coating prepared on aluminum plate by microarc oxidation. *Ceram. Int.* **2014**, *40*, 9981–9987. [CrossRef]
49. Hu, L.H.; Liu, X.R.; Wang, Q.X.; Zhou, Y. Highly efficient degradation of high-loaded phenol over $Ru\text{-}Cu/Al_2O_3$ catalyst at mild conditions. *RSC Adv.* **2017**, *7*, 21507. [CrossRef]
50. Leong, S.; Razmjou, A.; Wang, K.; Hapgood, K.; Zhang, X.; Wang, H. TiO_2 based photocatalytic membranes: A review. *J. Membr. Sci.* **2014**, *472*, 167–184. [CrossRef]
51. Zheng, Y.; Wang, Z.; Peng, F.; Wang, A.; Cai, X.; Fu, L. Growth of Cu_2O nanoparticle on reduced graphene sheets with high photocatalytic activity for degradation of Rhodamine B. *Full Nanotub. Carbon Nanostruct.* **2015**, *24*, 149–153. [CrossRef]
52. Ozawa, M.; Kimura, M.; Isogai, A. Thermal stability and characterization of $\gamma\text{-}Al_2O_3$ modified with lanthanum or cerium. *J. Mater. Sci. Lett.* **1990**, *9*, 709–711. [CrossRef]
53. Dong, C.; Zhong, M.; Huang, T.; Ma, M.; Wortmann, D.; Brajdic, M.; Kelbassa, I. Photodegradation of Methyl Orange under Visible Light by Micro-Nano Hierarchical Cu_2O Structure Fabricated by Hybrid Laser Processing and Chemical Dealloying. *ACS Appl. Mater. Interfaces* **2011**, *3*, 4332–4338. [CrossRef] [PubMed]
54. Zhou, X.Y.; Zhou, P.W.; Guo, H.; Yang, B.; Ren, R.F. Photocatalytic Activity of CuO/ZnO Heterostructure Nanocrystals under UV-Visible Light Irradiation. *Mater. Sci. Forum* **2014**, *787*, 35–40. [CrossRef]
55. Robles, M.R.G.; Bueno, J.D.J.P.; Syllas, C.S.A.; López, M.L.M.; Guerrero, F.M. Silver/Silicon nanowires/copper nanoparticles heterojunction for methyl orange degradation by heterogeneous photocatalysis under visible irradiation. *MRS Adv.* **2018**, *3*, 3933–3938. [CrossRef]